

# Spontaneous emission and spectral properties of radiation by relativistic electrons in a gyro-klystron and optical-klystron undulator

Bramha Prakash, Ganeswar Mishra\* and Roma Khullar

Insertion Device Development Laboratory, Department of Physics, Devi Ahilya University, Indore, Madhya Pradesh 452001, India. \*Correspondence e-mail: gmishra\_dauniv@yahoo.co.in

Received 11 July 2015

Accepted 23 December 2015

Edited by G. Grübel, HASYLAB at DESY, Germany

**Keywords:** undulator; klystron; gyrotron; undulator radiation.

In this paper spontaneous emission of radiation by relativistic electrons in a gyro-klystron is studied. The scheme consists of two solenoid sections separated by a dispersive section. In the dispersive section the electrons are made non-resonant with the radiation. The dispersive section transforms a small change of the velocity into changes of the phases of the electrons. This leads to enhanced radiation due to klystron-type modulation as compared with a conventional gyrotron-type device driven by cyclotron maser interaction. It is shown that the klystron-modulated spectrum depends on the dispersive field strength, finite perpendicular velocity component and length of the solenoids but is independent of the axial magnetic field strength. A simple scheme to design a gyro-klystron is discussed.

## 1. Introduction

There exists interest in free-electron lasers (FELs) (Margaritondo & Rebernick, 2011; McNeil & Thompson, 2010) and cyclotron resonance masers (Du & Liu, 2014; Bertolotti, 2015; Chu, 2004) as tunable light sources producing high-power coherent radiation over a wide wavelength range. In a FEL scheme, the relativistic electron beam travels through a wiggler/undulator field and undergoes transverse oscillations. The device operates both in amplifier and oscillator mode either through co-propagating laser light or with mirror. On the other hand, the relativistic electron beam with initial finite transverse velocity component travels in an axial magnetic field emitting coherent radiation *via* cyclotron resonance maser interaction. A comparison of both mechanisms has been discussed by many authors (Chu, 2004; Fruchtman, 1988; Danly *et al.*, 1992). The undulator is the key component of the FEL (Couprie, 2014) and has undergone several important improvements and modifications over the past decades and finds increasing applications in FELs and inverse free-electron lasers (IFELs). Studies on two-frequency undulators (Iracane & Bamas, 1991; Ciocci *et al.*, 1993), bi-harmonic undulators (Dattoli *et al.*, 2002, 2006; Kong *et al.*, 2000; Gupta & Mishra, 2006), variable-period undulators (Vinokurov *et al.*, 2011) and RF undulators (Kuzikov *et al.*, 2013) have been reported extensively in a number of physical configurations to exploit their novel properties for FEL and IFEL applications. In recent years there has been increased interest in the optical klystron undulator free-electron laser (OKFEL) for enhanced laser gain (Jain & Mishra, 2014; Freund, 2013). The OKFEL uses two sections of an undulator with a dispersive section in between. In the first section of the undulator, *i.e.* the modulator, the electron undergoes transverse oscillations and



accelerations. The dispersive section is either a three- or four-section chicane where the electrons experience modulation without resonant interaction. Without resonant interaction in the dispersive section, the small changes in the electron velocity lead to phase modulation and this leads to enhanced emission of radiation in the second section of the undulator, called the radiator (Dattoli & Bucci, 2000a,b; Dattoli *et al.*, 1993; Gehlot & Mishra, 2010; Elleaume, 1986; Kong, 1996). There have been several studies on the optical klystron undulator that explain the modelling of the dispersive section (Boscolo & Colson, 1985; Colson & Fredman, 1983; Gallardo & Pellegrini, 1990a,b; Thomas *et al.*, 2002; Elleaume, 1983; Vinokurov & Skrinisky, 1977; Vinokurov, 1977; Artamonov *et al.*, 1980).

In this paper we reconsider the theory of the optical klystron undulator to propose a gyro-klystron device where the two sections of solenoids producing the axial magnetic field are separated by a dispersive or drift section. The scheme is similar to an optical klystron undulator where the two undulator sections are replaced by solenoids. The two solenoid sections, having equal lengths and equal number of turns, are separated by a dispersive section. Fig. 1 illustrates the scheme. The electrons undergo cyclotron resonance oscillations in the modulator section, *i.e.*  $\omega \approx s\Omega_c$ , where  $\Omega_c$  is the relativistic cyclotron frequency. The dispersive section is considered as a section of the solenoid having a higher number of turns in order to have a large axial magnetic field. The large value of the axial magnetic field offsets the cyclotron resonance and allows the electrons to be phase modulated in correspondence with a change in velocity. In §2 the Lienard–Wiechert potential is solved and an analytical expression is derived for the gyro-klystron radiation. The results are discussed in §3. The analysis describes the spike pattern of the gyro-klystron radiation and compares it with the optical klystron undulator radiation. In an optical-klystron undulator the spikes depend on the number of undulator parameters, the undulator period and the undulator gap. In contrast, the spikes in the gyro-klystron depend on the finite perpendicular velocity component, the length of the solenoid and are independent of the solenoid magnetic field strength. In both cases the spikes vanish in the limit  $D \rightarrow 0$  ( $D$  is the dispersive field strength or the length of the drift section) and spikes become closer with increasing value of the dispersive field strength. Finally, a practical scheme is proposed for fabrication of the gyro-klystron with a discussion on optical klystron undulator radiation.

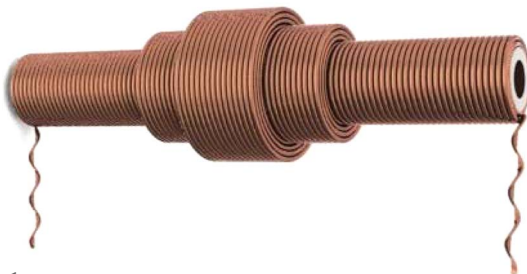


**Figure 1**  
Conceptual design of a three-section gyro-klystron device.

## 2. Gyro-klystron and optical klystron undulator radiation

The brightness is the energy radiated per solid angle per unit frequency and is evaluated from the Lienard–Wiechert potential (Jackson, 1962; Brau, 2004; Bosch, 1997),

$$\frac{d^2I}{d\Omega d\omega} = \frac{e^2\omega^2}{4\pi^2c} \left| \int_{-\infty}^{\infty} [\hat{n} \times (\hat{n} \times \vec{\beta})] \exp\left[i\omega\left(t - \frac{\hat{n} \cdot \vec{r}}{c}\right)\right] dt \right|^2, \quad (1)$$

where  $e$  is the electron charge,  $c$  is the velocity of light in a vacuum,  $\omega$  is the radiation frequency,  $\vec{r}$  is the electron trajectory and  $\hat{n}$  is an observation unit vector. In (1) the integral is carried from 0 to  $T$  where the electrons experience an effective acceleration, *i.e.*  $T = L/c\beta_z$ .  $\hat{n}$  is the observation unit vector with components  $\hat{n} = (\psi \cos \varphi, \psi \sin \varphi, 1 - \psi^2/2)$ , where  $\psi$  is the observation angle and  $\varphi$  is the azimuthal angle. We assume that the relativistic electron moves in a backward-propagating circularly polarized electromagnetic wave combined with an axial magnetic field described by

$$\begin{aligned} \vec{B}_u &= B_u [\cos(k_u z + \omega_u t), \sin(k_u z + \omega_u t), 0], \\ \vec{E}_u &= (\omega/c k_u) B_u [-\sin(k_u z + \omega_u t), \cos(k_u z + \omega_u t), 0], \\ \vec{B} &= \hat{z} B_0, \end{aligned} \quad (2)$$

where  $B_u$  is the amplitude of the wiggler magnetic field.  $\omega_u$ ,  $k_u$  are the frequency and the wavenumber of the electromagnetic wave wiggler, and  $B_0$  is the axial field. It is assumed that the axial field starts and ends abruptly on a length  $L = N\lambda_u$ ;  $\lambda_u$  is the period of the electromagnetic wave and  $N$  is the number of periods of the wave. The trajectory is provided by the Lorentz force equation,

$$\frac{d\vec{\beta}}{dt} = \frac{e}{\gamma mc} \left[ (\vec{\beta} \times \vec{B}_u) + (\vec{\beta} \times \hat{z} B_0) \right] + \frac{e\vec{E}_u}{\gamma mc}. \quad (3)$$

From (3) we write the equations of motion in transverse and longitudinal components,

$$\begin{aligned} \frac{d\beta_x}{dt} &= \frac{-eB_u\omega_u}{\gamma mck_u c} \sin(k_u z + \omega_u t) \\ &\quad - \frac{eB_u}{\gamma mc} \beta_z \sin(k_u z + \omega_u t) + \beta_y \Omega_c, \\ \frac{d\beta_y}{dt} &= \frac{eB_u\beta_z}{\gamma mck_u c} \cos(k_u z + \omega_u t) \\ &\quad + \frac{eB_u}{\gamma mc} \frac{\omega_u}{k_u c} \cos(k_u z + \omega_u t) - \beta_x \Omega_c, \\ \frac{d\beta_z}{dt} &= \frac{eB_u\beta_x}{\gamma mck_u c} \sin(k_u z + \omega_u t) \\ &\quad - \frac{eB_u\beta_y}{\gamma mc} \cos(k_u z + \omega_u t), \end{aligned} \quad (4)$$

where  $\Omega_c = eB_0/\gamma mc$  is the relativistic cyclotron frequency. The transverse equations in (4) can be now analytically solved from the initial condition that  $d\beta_z/dt = 0$ . The electron

transverse velocities from (4) are solved with a set of prescribed initial condition as

$$\begin{aligned}\beta_x &= \frac{K_c}{\gamma} \cos(\Omega t) + \left[ \beta_x(0) - \frac{K_c}{\gamma} \right] \cos(\Omega_c t), \\ \beta_y &= \frac{K_c}{\gamma} \sin(\Omega t) - \left[ \beta_y(0) - \frac{K_c}{\gamma} \right] \sin(\Omega_c t).\end{aligned}\quad (5)$$

The modified undulator parameter is defined as

$$K_c = \frac{eB_u}{mc^2 k_u} \left( \frac{1}{1+b} \right), \quad b = \left( \frac{\Omega_c}{\Omega} \right), \quad \Omega = \omega_u + k_u v_z,$$

where  $v_z$  is the electron longitudinal velocity, we assume  $\beta_x(0) = \beta_y(0) = \beta_\perp$ , and rewrite the transverse velocity components as

$$\begin{aligned}\beta_x &= \frac{K_c}{\gamma} \cos(\Omega t) + A \cos(\Omega_c t), \\ \beta_y &= \frac{K_c}{\gamma} \sin(\Omega t) - A \sin(\Omega_c t), \\ \beta_z &= \beta^* + \frac{K_c A}{\gamma} \cos[(\Omega + \Omega_c)t],\end{aligned}\quad (6)$$

where  $A = \beta_\perp - K_c/\gamma$ ,  $\beta^* = 1 - (1/2\gamma^2)(1 + K_c^2 + \gamma^2 A^2)$ . A further integration of (6) provides the electron trajectories as

$$\begin{aligned}x &= \frac{K_c}{\gamma \Omega} \sin(\Omega t) + \frac{A}{\Omega_c} \sin(\Omega_c t), \\ y &= \frac{-K_c}{\gamma \Omega} \cos(\Omega t) + \frac{A}{\Omega_c} \cos(\Omega_c t) \\ z &= \beta^* ct + \frac{c K_c A}{\gamma(\Omega + \Omega_c)} \sin[(\Omega + \Omega_c)t].\end{aligned}\quad (7)$$

The scalar product  $\hat{n} \cdot \vec{r}$  in equation (1) on-axis reads as

$$\hat{n} \cdot \vec{r}|_{\psi=0} = \beta^* ct + \frac{K_c A}{\gamma(\Omega + \Omega_c)} \sin[(\Omega + \Omega_c)t]. \quad (8)$$

The cross product in equation (1) is evaluated on-axis as

$$\left[ \hat{n} \times (\hat{n} \times \vec{\beta}) \right]_j = -\beta_j, \quad \psi = 0, \quad j = x, y. \quad (9)$$

Equations (8) and (9) can be combined to evaluate the exponential term as

$$\exp \left\{ i\omega \left( t - \frac{\hat{n} \cdot \vec{r}}{c} \right) \right\} = \sum_{m=-\infty}^{\infty} \exp \left\{ \left[ \frac{i\omega}{\omega_1} - im(\Omega + \Omega_c) \right] t \right\} J_m(\xi), \quad (10)$$

where  $\xi = \omega K_c A / [\gamma(\Omega + \Omega_c)]$ ,  $\omega_1 = 2\gamma^2 / (1 + K_c^2 + \gamma^2 A^2)$  and  $J_m(\xi)$  is the cylindrical Bessel function of the first kind of the  $m$ th order. We now define the intensity components of the radiation spectrum as

$$T^j = \int_{-\infty}^{\infty} \left[ \hat{n} \times (\hat{n} \times \vec{\beta}) \right]_j \exp \left[ i\omega \left( t - \frac{\hat{n} \cdot \vec{r}}{c} \right) \right] dt, \quad j = x, y. \quad (11)$$

Equations (9) and (10) can be used now to solve equation (11). In (11), the limits of the integral for a klystron-type device can be written as

$$\int_{-\infty}^{\infty} dt(\dots) = \int_0^T dt(\dots) + \int_{T(1+D)}^{T(2+D)} dt(\dots). \quad (12)$$

$T = L/c$ , where  $L$  is the length of the solenoid for the gyro-klystron;  $L = N\lambda_u$  for the optical klystron undulator where  $\lambda_u$  is the wavelength of the electromagnetic wave wiggler. We consider the interaction in a klystron field configuration with a dispersive section ‘ $D$ ’ in between the two sections, where  $D = L_d/L$  is the dimensionless parameter of the dispersive section,  $L_d$  is the length of the dispersive section and  $L$  is the length of two modulator/radiator sections. The energy radiated per unit solid angle and per unit frequency interval can now be written as

$$\frac{d^2 I}{d\omega d\Omega} = \frac{e^2 \omega^2 T^2}{4\pi^2 c} [ |T^x|^2 + |T^y|^2 ], \quad (13)$$

where

$$\begin{aligned}T^x &= - \left[ \frac{K_c}{2\gamma} J_m(\xi) + \frac{A}{2} J_{m-1}(\xi) \right] H_2 \\ &\quad - \left[ \frac{A}{2\gamma} J_m(\xi) + \frac{K_c}{2\gamma} J_{m-1}(\xi) \right] H_1, \\ T^y &= - \left[ \frac{K_c}{2i\gamma} J_m(\xi) + \frac{A}{2i} J_{m-1}(\xi) \right] H_2 \\ &\quad + \left[ \frac{A}{2i\gamma} J_m(\xi) + \frac{K_c}{2i\gamma} J_{m-1}(\xi) \right] H_1.\end{aligned}\quad (14)$$

In (14),  $H_1$  and  $H_2$  are the line-shape integrals where

$$\begin{aligned}|H_1|^2 &= T^2 \frac{\sin^2(\nu_1 T/2)}{(\nu_1 T/2)^2} \left[ 2 + 2 \cos \nu_1 T(1 + D) \right], \\ \nu_1 &= \left[ \frac{\omega}{\omega_1} - (m-1)\Omega_c - m\Omega \right], \\ |H_2|^2 &= T^2 \frac{\sin^2(\nu_2 T/2)}{(\nu_2 T/2)^2} \left[ 2 + 2 \cos \nu_2 T(1 + D) \right], \\ \nu_2 &= \left[ \frac{\omega}{\omega_1} - (m-1)\Omega - m\Omega_c \right].\end{aligned}\quad (15)$$

### 3. Results and discussion

In this paper we have discussed spontaneous emission of radiation of relativistic electrons in a field configuration that consists of an electromagnetic wiggler and an axial magnetic field. The electron motion has been discussed and an analytical expression has been derived from the Lienard–Wiechert potential in the far-field limit. In the case where  $K_c = 0$  (in the absence of the electromagnetic wiggler) the scheme is the gyro-klystron device where two solenoid sections are separated by a dispersive section. The scheme with a three-section dispersive region is illustrated in Fig. 1. In this scheme we derive the Lienard–Wiechert potential expression from equation (14) and obtain

$$\begin{aligned} T^x &= \left[ \frac{\beta_{\perp}}{2} J_{m-1}(0) \right] H_2 - \left[ \frac{\beta_{\perp}}{2\gamma} J_m(0) \right] H_1, \\ T^y &= - \left[ \frac{\beta_{\perp}}{2i} J_{m-1}(0) \right] H_2 + \left[ \frac{\beta_{\perp}}{2i} J_m(0) \right] H_1. \end{aligned} \quad (16)$$

There is fundamental emission of radiation corresponding to  $m = 1$  and we obtain

$$\begin{aligned} T^x &= \left[ \frac{\beta_{\perp}}{2} J_{m-1}(0) \right] H_2, \\ T^y &= - \left[ \frac{\beta_{\perp}}{2i} J_{m-1}(0) \right] H_2, \quad v_2 = \left[ \frac{\omega}{\omega_1} - \Omega_c \right]. \end{aligned} \quad (17)$$

In Fig. 2 we plot the intensity from the gyro-klystron radiation with finite perpendicular velocity component as the parameter, *i.e.*  $\beta_{\perp} = 0.10, 0.08, 0.06$ . The other parameters are  $\gamma = 10, L = 50$  cm,  $D = 2$  and  $B = 10$  kG. In the first solenoid section the electrons execute larmor motion with larmor orbit given by  $r_L = c\beta_{\perp}/\omega_c$ . As the electron enters the dispersive region ( $D$  section) the axial magnetic field is increased to detune the resonant interaction. This enables the electron to increase its  $c\beta_{\perp}$  values so that the larmor orbit ( $c\beta_{\perp}/\omega_c$ ) and the magnetic moment ( $mc^2\beta_{\perp}^2/2B_0$ ) of the electron remain constant. The magnetic moment is a constant of motion in a slowly varying magnetic field. As a consequence the electron longitudinal velocity becomes modulated as the total electron energy ( $mc^2\beta_{\perp}^2/2 + mc^2\beta_{\parallel}^2/2$ ) is constant. The electron longitudinal velocity modulation introduces phase modulation analogous to an optical-klystron undulator scheme. The electron possessing a higher initial perpendicular velocity component offers more intensity than the electron possessing lower perpendicular velocity due to azimuthal bunching inherent to a gyro-device. In Fig. 3 the spectral properties of the gyro-klystron radiation are clarified with beam energy as the parameter. The radiation is maximum at  $\beta_{\perp}\gamma \approx 1$ . The full width at half-maximum is another important spectral property. For the gyro-klystron it is easy to see that

$$(\Delta\omega)_{\text{FWHM}} = \pm 1.3916 \left( \frac{4\gamma^2}{1 + \gamma^2\beta_{\perp}^2} \right) \frac{c\beta_z}{L}. \quad (18)$$

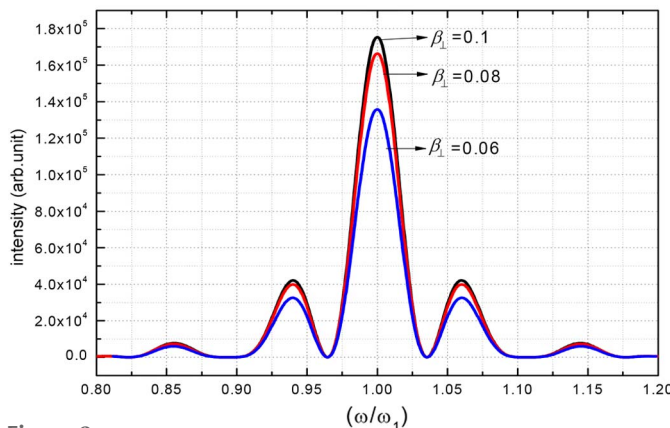


Figure 2 Gyro-klystron radiation *versus* frequency.

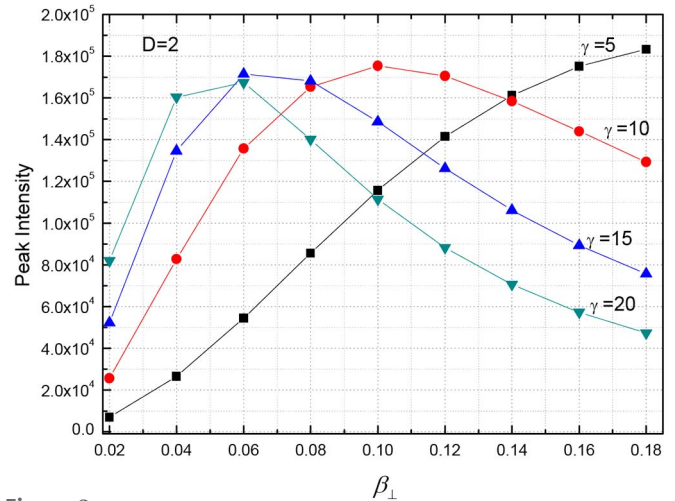


Figure 3 Peak intensity *versus* perpendicular velocity.

In Fig. 4 the intensity is plotted for several values of the dispersive field strengths ( $D$  values). Similar to optical-klystron undulator radiation, the gyro-klystron radiation is characterized by spikes in the radiation spectrum. The spikes occur at zeros of the modulating cosine function in equation (15),

$$\omega - \omega_0 = \pm \frac{n\pi}{2} \frac{4\gamma^2}{1 + \gamma^2\beta_{\perp}^2} \left[ \frac{c\beta_z}{L(1 + D)} \right]. \quad (19)$$

$\omega_0$  is the central peak of the radiation and  $n$  is the zeros of the cosine function. For increasing values of the dispersive field strengths, micro-bunching increases, increasing the number of spikes. The peak intensity *versus* perpendicular velocity is plotted in Fig. 5 for several values of  $D$ . The  $D$  values are varied from  $D = 2$  to  $D = 6$ . The plots give an important insight that the peak intensity occurs at  $\beta_{\perp}\gamma \approx 1$  irrespective of the increased  $D$  values. The frequency widths of the spikes *versus*  $D$  are analyzed in Fig. 6. For lower  $\beta_{\perp}$  values the frequency widths between spikes are wider than for the beams with

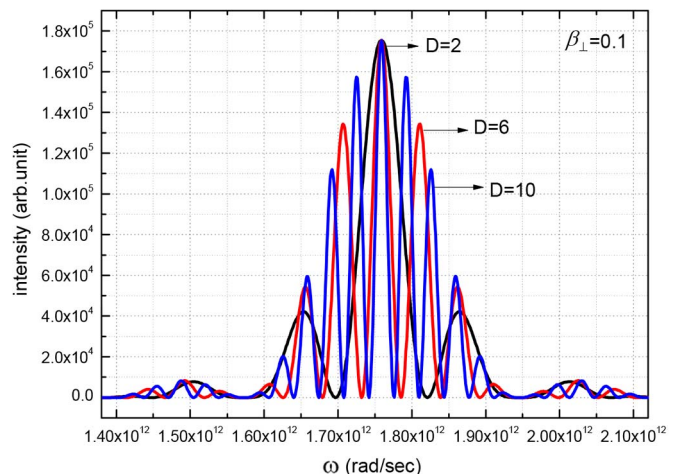
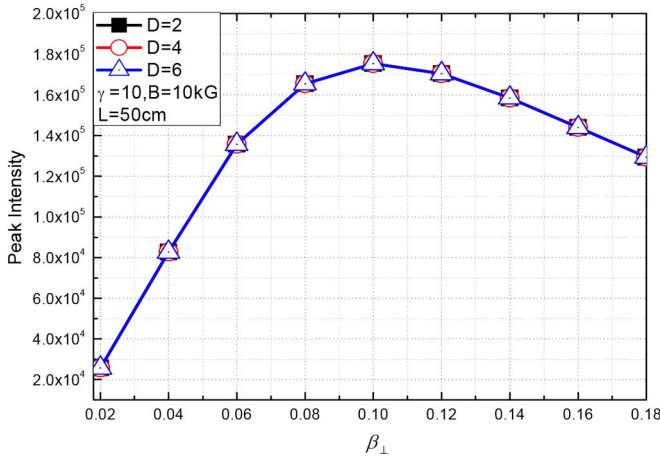


Figure 4 Gyro-klystron spectrum.



**Figure 5**  
Peak intensity versus perpendicular velocity for several values of  $D$ .

higher  $\beta_{\perp}$ . Higher  $\beta_{\perp}$  values give stronger micro-bunching due to klystron-type interactions which are further enhanced for higher  $D$  values. In the case of the electromagnetic wiggler pumped optical-klystron, the intensity reads, from equation (14), as

$$\begin{aligned} T^x &= -\left[\frac{K}{2\gamma} J_m(0)\right] H_2 - \left[\frac{K}{2\gamma} J_{m-1}(0)\right] H_1, \\ T^y &= -\left[\frac{K}{2i\gamma} J_m(0)\right] H_2 + \left[\frac{K}{2i\gamma} J_{m-1}(0)\right] H_1. \end{aligned} \quad (20)$$

There is fundamental emission of radiation corresponding to  $m = 1$  and we obtain

$$\begin{aligned} T^x &= -\left[\frac{K}{2\gamma} J_{m-1}(0)\right] H_1 \\ T^y &= \left[\frac{K}{2i\gamma} J_{m-1}(0)\right] H_1, \quad v_1 = \left[\frac{\omega}{\omega_1} - \Omega\right]. \end{aligned} \quad (21)$$

The optical-klystron undulator radiation characteristics can be obtained from gyro-klystron expressions when we use  $K/\gamma = \beta_{\perp} L$ ,  $L = N\lambda_u$  and  $\beta_z = 1$ .

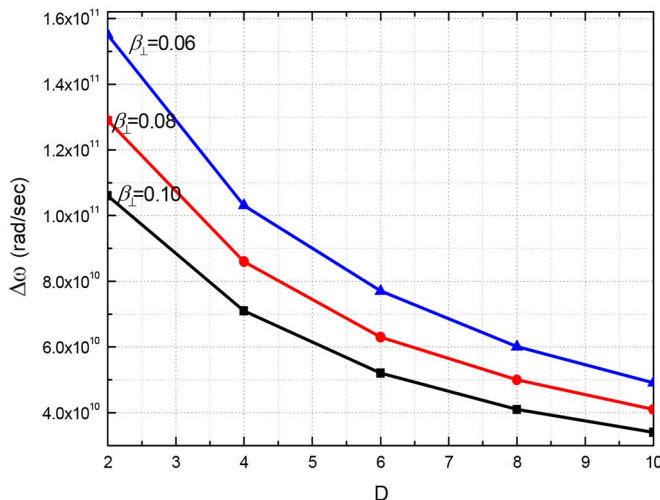


**Figure 6**  
Frequency width versus  $D$  for different values of  $\beta_{\perp}$ .

In conclusion, this paper has put forward a conceptual design structure of a gyro-klystron device. A simple analytical expression of the Lienard–Wiechert potential expression is derived and several characteristics of the gyro-klystron radiation have been analyzed and discussed. The fabrication of the gyro-klystron can be made from knowledge of the axial magnetic field in a solenoid, given by  $B(T) = \mu_r \mu_0 NI/l$ , where  $\mu_r$  is the relative permittivity,  $I$  is the current in the wire in amperes,  $\mu_0$  is the free-space permittivity and is given by  $\mu_0 = 4\pi \times 10^{-7} T - m/A$ ,  $l$  is the length,  $N$  is the number of turns and  $N/l$  is the turn density. There is no dependence on the diameter of the solenoid. The field inside the solenoid does not depend on the position inside the solenoid, *i.e.* the field at any longitudinal position is constant. These facts can be used to fabricate the solenoid for the gyro-klystron. A scheme of the three-chicane dispersive section is shown in Fig. 1. A simple scheme is to keep the applied current constant while varying the number of turns to increase the magnetic field in the dispersive section. Alternately the dispersive section can be an independent unit. For, example if we consider  $I = 50$  A,  $N = 16$ ,  $l = 0.5$  m and  $\mu_r = 200$  (iron), we obtain  $B = 0.4$  T. If the number of turns in the dispersive section is increased to  $N = 80$ , we obtain  $B = 2$  T. A second option would be to fabricate the dispersive section with mu-material whose relative permittivity is several times higher than that of iron. The analytical results are obtained from the far-field expression of the Lienard–Wiechert potential in equation (1). In the far-field limit the acceleration fields are large compared with the velocity fields and are retained in the expression for the Lienard–Wiechert potential (Jackson, 1962; Brau, 2004; Bosch, 1997). The validity of the far-field expression has been examined in detail by Bosch (1997). For example, in this paper we have considered an electron beam kinetic energy of  $\gamma = 10$ . For a magnetic field of  $B_0 = 10$  kG = 1.0 T and using  $f_c = 28$  GHz  $T^{-1}$  and wavelength of radiation 1.07 mm, the application of the far-field approximation requires  $R \gg \lambda\gamma^2$ . This gives  $R \gg 107$  mm (Bosch, 1997).

### Acknowledgements

The authors are grateful to Dr Markus Tischer, DESY, Germany, and Dr Marie-Emmanuelle Couprie, Soleil, France, for many technical discussions and input on undulator technology during the Science and Technology of Free-Electron Lasers workshop on 4–6 December 2014 at DAVV, Indore, India. This work is financially supported by SERB, DST, Delhi, Government of India, through a grant No. EMR /2014/ 000120.

### References

- Artamonov, A. S., Vinokurov, N. A., Voblyi, P. D., Gluskin, E. S., Korniyukhin, G. A., Kochubei, V. A., Kulipanov, G. N., Litvinenko, V. N., Mezentsev, N. A. & Skrinsky, A. N. (1980). *Nucl. Instrum. Methods*, **177**, 247–252.
- Bertolotti, M. (2015). *Masers and Lasers: A Historical Approach*, 2nd ed. CRC Press.
- Bosch, R. A. (1997). *Nucl. Instrum. Methods Phys. Res. A*, **386**, 525–530.

- Boscò, I. & Colson, W. B. (1985). *Nucl. Instrum. Methods Phys. Res. A*, **237**, 118–123.
- Brau, C. A. (2004). *Modern Problems in Classical Electrodynamics*. Oxford University Press.
- Chu, K. R. (2004). *Rev. Mod. Phys.* **76**, 489–540.
- Ciucci, F., Dattoli, G., Giannessi, L., Torre, A. & Voykov, G. (1993). *Phys. Rev. E*, **47**, 2061.
- Colson, W. B. & Fredman, R. A. (1983). *Phys. Rev. A*, **27**, 1399.
- Coupré, M. E. (2014). *J. Electron Spectrosc. Relat. Phenom.* **196**, 3–13.
- Danly, B. G., Hartemann, F. V., Chu, T. S., Legorburu, P., Menninger, W. L., Temkin, R. J., Faillon, G. & Mourier, G. (1992). *Phys. Fluids B*, **4**, 2307.
- Dattoli, G. & Bucci, L. (2000a). *Nucl. Instrum. Methods Phys. Res. A*, **450**, 479–490.
- Dattoli, D. & Bucci, L. (2000b). *Opt. Commun.* **177**, 323–331.
- Dattoli, D., Galli, M., Ottaviani, P. L. & Torre, A. (1993). *Nucl. Instrum. Methods Phys. Res. A*, **333**, 589–593.
- Dattoli, G., Giannessi, L., Ottaviani, P. L., Freund, H. P., Biedron, S. G. & Milton, S. (2002). *Nucl. Instrum. Methods Phys. Res. A*, **495**, 48–57.
- Dattoli, G., Mikhailin, V. V., Ottaviani, P. L. & Zhukovsky, K. V. (2006). *J. Appl. Phys.* **100**, 084507.
- Du, C.-H. & Liu, K.-P. (2014). *Millimeter-Wave Gyrotron Traveling-Wave Tube Amplifiers*. Berlin/Heidelberg: Springer-Verlag.
- Elleaume, P. (1983). *J. Phys. Colloq.* **44**, C1-333–C1-352.
- Elleaume, P. (1986). *Nucl. Instrum. Methods Phys. Res. A*, **250**, 220–227.
- Freund, H. P. (2013). *Phys. Rev. ST Accel. Beams*, **16**, 060701.
- Fruchtman, A. (1988). *Phys. Rev. A*, **37**, 4252–4258.
- Gallardo, J. C. & Pellegrini, C. (1990a). *Nucl. Instrum. Methods Phys. Res. A*, **296**, 448–450.
- Gallardo, J. C. & Pellegrini, C. (1990b). *Opt. Commun.* **77**, 45–48.
- Gehlot, M. & Mishra, G. (2010). *Opt. Commun.* **283**, 1445–1448.
- Gupta, V. & Mishra, G. (2006). *Nucl. Instrum. Methods Phys. Res. A*, **556**, 350–356.
- Iracane, D. & Bamas, P. (1991). *Phys. Rev. Lett.* **67**, 3086–3089.
- Jackson, J. D. (1962). *Classical Electrodynamics*. New York: Wiley.
- Jain, D. & Mishra, G. (2014). *Nucl. Instrum. Methods Phys. Res. A*, **767**, 75–82.
- Kong, M. G. (1996). *Opt. Commun.* **132**, 464–468.
- Kong, M. G., Zhong, X. & Vourdas, A. (2000). *Nucl. Instrum. Methods Phys. Res. A*, **445**, 7–12.
- Kuzikov, S. V., Jiang, Y., Marshall, T. C., Sotnikov, G. V. & Hirshfield, J. L. (2013). *Phys. Rev. ST AB*, **16**, 070701.
- McNeil, B. W. J. & Thompson, N. R. (2010). *Nat. Photon.* **4**, 814.
- Margaritondo, G. & Rebernik Ribic, P. (2011). *J. Synchrotron Rad.* **18**, 101–108.
- Thomas, C. A., Botman, J. I. M., Van de Geer, B. & de Loos, M. (2002). *Proceedings of the Eighth European Particle Accelerator Conference (EPAC'2002)*, Paris, France, pp. 842–845.
- Vinokurov, N. A. (1977). *Proceedings of the Xth International Conference on High Energy Charged Particle Accelerators*, Serpukov, USSR, Vol. 2, p. 454.
- Vinokurov, N. A., Shevchenko, O. A. & Tcheskidov, V. G. (2011). *Phys. Rev. ST Accel. Beams*, **14**, 040701.
- Vinokurov, N. A. & Skrinsky, A. N. (1977). PrePrint INP 77–59, Novosibirsk.